

Design constraints and guidelines for CdS/CdTe nanopillar based photovoltaics

Rehan Kapadia, Zhiyong Fan, and Ali Javey^{a)}

Department of Electrical Engineering and Computer Sciences, University of California at Berkeley, Berkeley, California 94720, USA; Berkeley Sensor and Actuator Center, University of California at Berkeley, Berkeley, California 94720, USA; and Materials Sciences Division, Lawrence Berkeley National Laboratory, Berkeley, California 94720, USA

(Received 13 January 2010; accepted 9 February 2010; published online 11 March 2010)

The performance dependence of a CdS/CdTe nanopillar solar cell on various device and materials parameters is explored while examining its performance limits through detailed device modeling. The optimized cell enables efficiencies $> \sim 20\%$ with minimal short circuit current dependence on bulk minority carrier diffusion length, demonstrating the efficient collection of photogenerated carriers, therefore, lowering the materials quality and purity constraints. Given the large p - n junction interface area, the interface recombination velocity is shown to have detrimental effect on the device performance of nanopillar solar cells. In that regard, the CdS/CdTe material system is optimal due to its low interface recombination velocity. © 2010 American Institute of Physics. [doi:10.1063/1.3340938]

Over the past several years, nanostructured materials have been extensively explored for photovoltaic (PV) devices. Specifically, nanowire (NW) and nanopillar (NPL) devices have been studied experimentally and computationally.¹⁻³ Recently, we reported a CdS/CdTe solar nanopillar (SNOP) cell with $\sim 6\%$ conversion efficiency, which despite nonoptimal contacts,³ is the highest efficiency arrayed NW/NPL cell reported.^{4,5} This performance advance is attributed to the proper use of device architecture and material system. Here, we explore the effects of materials quality and interface properties on the performance of CdS/CdTe SNOP cells through detailed device simulation while examining their performance limits.

The SNOP cell (Fig. 1(a)) consists of an array of CdS NPLs partially embedded in a CdTe thin film. The n-CdS NPLs serve as electron collectors, while the CdTe thin film serves as the absorber layer. Sentaurus Device 2009 was used to simulate the performance of these cells by solving Poisson's, and the electron and hole continuity equations self-consistently. Auger and Shockley-Read-Hall (SRH) recombination process were considered. The SRH recombination was assumed to be due to a single midgap trap level. Since Auger recombination in the CdTe film was orders of magnitude lower than SRH, the carrier lifetimes were set by controlling the SRH lifetime. To represent the effect of CdS/CdTe interface quality, interfacial SRH recombination through a midgap trap state was set by defining an interfacial recombination velocity (S_i) at the CdS/CdTe interface. The top and bottom contacts are assumed to be ohmic. In practice, however, there is generally a Schottky barrier at the metal contacts. The effect of this barrier is often modeled as a diode opposing the p - n junction of the device, resulting in degradation of fill factor and the open circuit voltage. The AM1.5g spectrum was simulated by binning the energy within the $0.831 \mu\text{m}$ to $0.32 \mu\text{m}$ range into 25 discrete wavelengths. The absorption for each wavelength was then calculated using a Beer's law model with the appropriate absorption coefficient.

The SNOP cell is simulated by defining half of a two-dimensional cross section of the device [Fig. 1(b)] and then assuming cylindrical symmetry in the device equations, using a scheme previously used for Si core/shell NW cells.² However, the simulated SNOP cell consisted of a square lattice of NPLs embedded in a CdTe film. This gives rise to a square "unit cell" as shown in Fig. 1(c), which is not accurately represented by the cylindrical structure in Fig. 1(b). Thus, to simulate the results for a SNOP-cell with a given pitch, multiple simulations with fixed NPL radius and increasing outer radius were simulated as shown in Fig. 1(c). The parameters of the SNOP cell were then calculated using the formula: $p = p(r_1) - \sum A(r_i, r_{i+1}) [p(r_i) - p(r_{i+1})] / [\pi r_{i+1}^2 - \pi r_i^2]$; where p represents the parameter of interest (i.e., conversion efficiency, η , open circuit voltage, V_{oc} , or photocurrent, J_{sc}), $p(r_1)$ is the parameter evaluated at radius r_1 , $A(r_i, r_{i+1})$ is the area bounded by circles of radius r_i , r_{i+1} , and the square. This approximation corrects for the missing area through the 1st order Taylor expansion terms from each of the larger diameter simulations. It should be noted that this result is only valid when the junctions are sufficiently far apart such that their depletion regions do not interact.

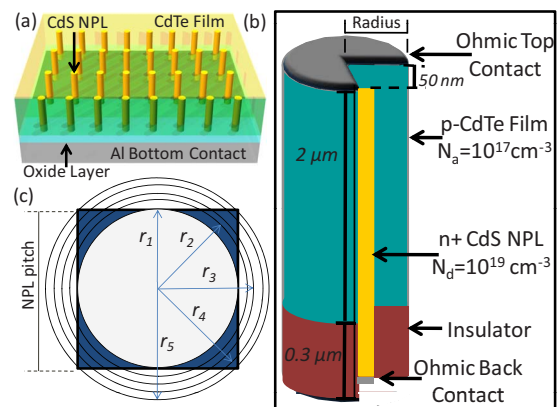


FIG. 1. (Color online) (a) Schematic of a SNOP-cell. (b) The structure used for device modeling after assuming cylindrical symmetry. (c) An overhead view of the unit cell.

^{a)}Electronic mail: ajavey@eecs.berkeley.edu.

The CdS NPL and CdTe thin film doping concentrations were set to $N_d=10^{19} \text{ cm}^{-3}$ and $N_a=10^{17} \text{ cm}^{-3}$, respectively. The CdS is highly doped to minimize parasitic resistance since it simply serves as an electron collector with minimal carrier generation. The CdTe doping concentration was chosen in order to maintain a moderate depletion region width of $\sim 60 \text{ nm}$ and still allow for accurate simulation of the device. The electron and hole mobilities used for CdS were $\mu_n=100 \text{ cm}^2/\text{V s}$ and $\mu_p=25 \text{ cm}^2/\text{V s}$, respectively.⁶ For CdTe, $\mu_n=100 \text{ cm}^2/\text{V s}$ and $\mu_p=40 \text{ cm}^2/\text{V s}$ were chosen as a median from the spread of values reported in literature.^{7,8} The minority carrier diffusion lengths were set by varying the SRH lifetime. In CdS, the hole diffusion length was fixed at $L_{p,\text{CdS}}=0.4 \text{ }\mu\text{m}$.⁹ Since the CdS contribution to the photocurrent is negligible, $L_{p,\text{CdS}}$ is not a critical parameter. For CdTe, a range of electron diffusion lengths, $L_{n,\text{CdTe}}=0.25\text{--}5 \text{ }\mu\text{m}$, was chosen, as these represent the lower and upper bounds for CdTe thin films.¹⁰ The thickness of the CdTe layer was set to $2 \text{ }\mu\text{m}$, corresponding to absorption of $\sim 85\%$ for an AM1.5 spectrum.¹¹ A $0.3 \text{ }\mu\text{m}$ thick insulator separates the bottom contact from the CdTe layer [Fig. 1(b)], and the NPL radius and pitch was chosen to be 0.1 and $0.5 \text{ }\mu\text{m}$, respectively.

Although there is significant emphasis on the effects of top surface and metal contact recombination processes on planar cells,¹² these effects have been poorly studied for the nanostructured cells. In the CdS/CdTe SNOP cell, only the top contact (i.e., CdTe/contact interface) contributes to the minority carrier loss since minimal light absorption takes place in the CdS NPLs. To determine the effect of contact recombination velocity (S_c) on SNOP cell performance, the structure in Fig. 1 was simulated with $S_i=10^3 \text{ cm/s}$, a typical experimentally measured value.¹³ S_c was then varied to represent a range of shielding qualities, from heavily shielded (10^2 cm/s) to unshielded (10^7 cm/s). The η shows a strong dependence on S_c [Fig. 2(a)], dropping $\sim 1.5\times$ and $1.3\times$ for $L_{n,\text{CdTe}}=0.25$ and $5 \text{ }\mu\text{m}$, respectively, as the S_c is increased from 10^2 to 10^7 cm/s . This efficiency drop is predominantly due to the degradation of J_{sc} [Figs. 2(b) and 2(c)], which is an indicator of the aggregate minority carrier collection efficiency. Interestingly, J_{sc} shows minimal dependence on $L_{n,\text{CdTe}}$ for the SNOP-cells, in distinct contrast to the planar cells. This trend is expected since for the SNOP-cell geometry explored here, all excess minority carriers are generated $<L_{n,\text{CdTe}}$ from the CdS/CdTe interface, resulting in their efficient collection. For all further simulations, a 5 nm thick region of $N_a=10^{19} \text{ cm}^{-3}$, which is an upper experimental limit for CdTe doping,¹⁴ directly under the top contact is used as a reflector. The reflector reduces the effect of contact recombination by shielding the minority carriers from the contacts through a potential barrier. When $S_c=10^7 \text{ cm/s}$ is enforced at the top contact, the reflector increases the performance of the cell to that of one with a $S_c \sim 10^4 \text{ cm/s}$, as confirmed by simulation, which effectively removes the impact of contact recombination on the cell performance [Fig. 2(a)]. It should be noted that in terms of contact recombination, SNOP-cell geometry presents an important advantage over coaxial NW cells since the planar contact of the SNOP-cells has significantly lower surface area (equivalent to that of the planar cells).

Due to the enhanced CdS/CdTe interfacial area of the SNOP-cell, the interface recombination processes can sig-

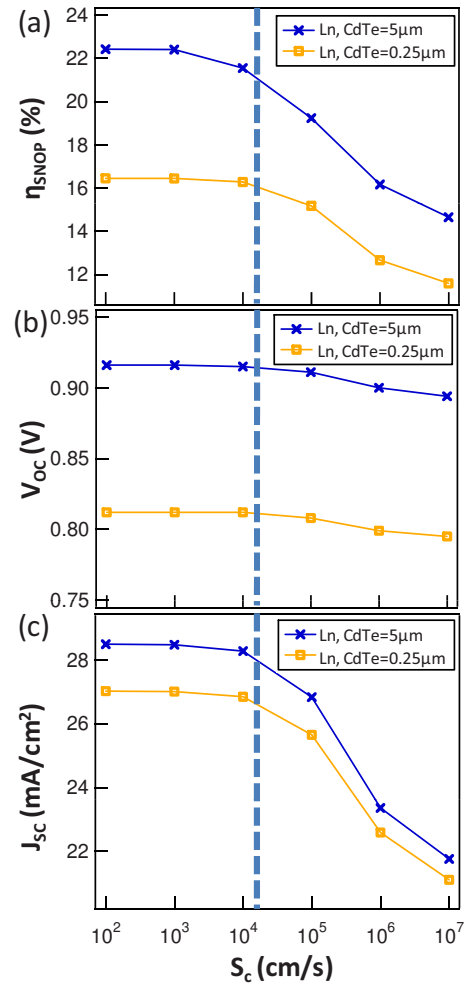


FIG. 2. (Color online) S_c dependency of (a) η , (b) V_{oc} , and (c) J_{sc} are shown for $S_i=10^3 \text{ cm/s}$ and $L_{n,\text{CdTe}}=0.25$ and $5 \text{ }\mu\text{m}$. The dashed lines represent the “effective” S_c when a 5 nm p+electron reflector is added under the top contact with $S_c=10^7 \text{ cm/s}$.

nificantly alter the device performance. The effect of interface quality on the device performance is modeled for $S_i=1\text{--}10^6 \text{ cm/s}$. Within this range, the interface recombination is found to affect the efficiency only when the bulk recombination rates are relatively low [Fig. 3(a)]. Specifically, we observed $\eta \sim 15\%$ with minimal S_i dependency for $L_{n,\text{CdTe}}=0.25 \text{ }\mu\text{m}$. On the other hand, when $L_{n,\text{CdTe}}=5 \text{ }\mu\text{m}$, the efficiency is reduced from $\sim 20\%$ to $\sim 16\%$ as the S_i is increased from $1\text{--}10^6 \text{ cm/s}$ [Fig. 3(a)]. The primary effect of enhanced S_i is a reduction in V_{oc} [Fig. 3(b)] with the J_{sc} being nearly constant [Fig. 3(c)]. For thin film CdS/CdTe, $S_i=10\text{--}10^3 \text{ cm/s}$ has been previously measured and reported in the literature.¹³ As a result, the CdS/CdTe material system is optimal for the SNOP-cell due to its low interface recombination velocity.

A simple analysis of the results can be carried out by defining an effective carrier lifetime, $1/\tau_{\text{eff}}=1/\tau_0+1/\tau_c+1/\tau_i$, where τ_0 is the bulk lifetime, τ_c is the lifetime due to recombination at the top contact, and τ_i is the lifetime due to interfacial recombination. To calculate τ_c and τ_i , S_c and S_i are first changed to equivalent surface trap densities, $N_{s,c}$ and $N_{s,i}$, respectively. This is achieved by using the relations $S_c=N_{s,c} \times \sigma \times v_{th}$, $S_i=N_{s,i} \times \sigma \times v_{th}$, and $\tau=1/(N_t \times \sigma \times v_{th})$, where σ is the capture cross section, v_{th} is the thermal velocity, and N_t is the trap density for a given volume. By assuming the surface traps are spread uniformly over a vol-

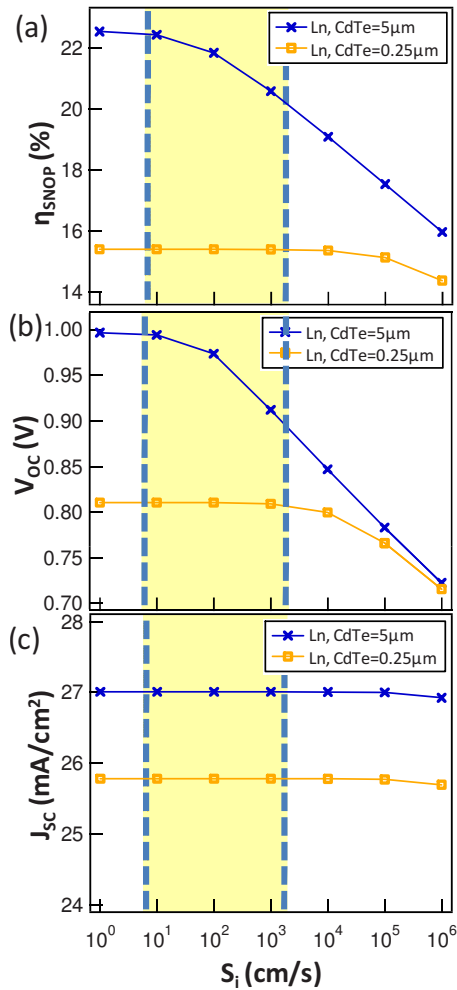


FIG. 3. (Color online) S_i dependency of (a) η , (b) V_{oc} , and (c) J_{sc} are shown for $S_c=10^7$ cm/s with a 5 nm p+electron reflector under the top contact, and $L_{n,CdTe}=0.25$ and $5 \mu\text{m}$. The experimentally reported range for S_i is highlighted for each graph.

ume, τ_c and τ_i can be approximated from the recombination velocities. For interface recombination, the appropriate volume would be the depletion region. On the other hand, the contact recombination affects minority carriers within $L_{n,CdTe}$ of the surface, unless the CdTe thickness is $<L_{n,CdTe}$, in which case it affects carriers through the entire film. This leads to the relation: $1/\tau_{eff}=1/\tau_0+S_c/L_{n,CdTe}+S_i/W_d$. For the case of $L_{n,CdTe}=5 \mu\text{m}$, $\tau_0=9.6 \times 10^{-8}$ s, and for $L_n=0.25 \mu\text{m}$, $\tau_0=2.4 \times 10^{-10}$ s. This indicates that, for $L_n=5 \mu\text{m}$ and with a p+reflector, the performance is limited by the interface recombination when $S_i > \sim 10^2$ cm/s. For $L_n=0.25 \mu\text{m}$, the interface recombination is dominant when $S_i > \sim 2 \times 10^4$ cm/s. This is clearly visible from Fig. 3, and indicates that this simple analysis is valid for estimating the dominant recombination processes in a SNOP cell, given the known material properties.

The effect of pitch on the performance of the SNOP cells was simulated by holding fixed the NPL radius while varying the pitch from 350 nm to $1 \mu\text{m}$. The simulation structure was the same as that show in Fig. 1, using $S_i=10^3$ cm/s, $S_c=10^7$ cm/s, and a 5 nm thick minority carrier reflector (i.e., effective $S_c \sim 10^4$ cm/s). The data shows two key trends: (i) as the diffusion length increases, the optimal pitch increases, and (ii) even for a system with a moderate diffusion length of $0.25 \mu\text{m}$, proper NPL pitch can enable re-

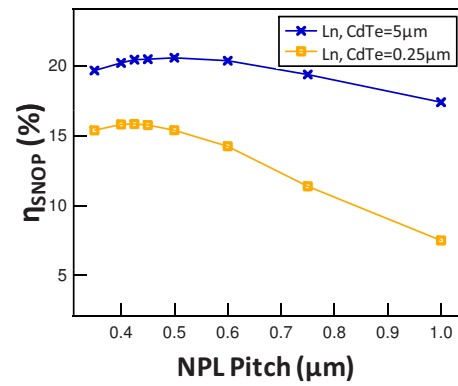


FIG. 4. (Color online) A plot of efficiency vs NPL pitch for $L_{n,CdTe}=0.25$ and $5 \mu\text{m}$. $S_i=10^3$ cm/s, $S_c=10^7$ cm/s with a 5 nm p+top contact electron reflector.

spectable efficiencies of 16% (Fig. 4). These results can be explained as a competition between the CdTe filling factor (i.e., the amount of the absorber layer), and the reduction in carrier collection efficiency with increased pitch. For lower quality materials, η is highly sensitive to NPL spacing and must be considered carefully for cell optimization. The median reported experimental value of minority carrier lifetimes¹⁵ in polycrystalline CdTe films correspond to diffusion lengths of $\sim 0.5 \mu\text{m}$, further indicating the importance of the SNOP geometry with optimized NPL pitch for the CdS/CdTe material system.

In conclusion, the projected performance limits of CdS/CdTe SNOP-cells are explored by examining the effects of various materials and device parameters on the conversion efficiency, showing that $\eta > \sim 20\%$ should be attainable through materials and device optimization. This work presents an important guideline for future experimental work, and highlights the importance of direct measurement of various recombination rates of nanopillar structures to further advance the efficiency of the cells; an area that has been poorly explored to date.

This work was supported by Berkeley Sensor and Actuator Center. R.K acknowledges an NSF Graduate Fellowship.

- ¹E. C. Garnett and P. D. Yang, *J. Am. Chem. Soc.* **130**, 9224 (2008).
- ²M. D. Kelzenberg, M. C. Putnam, D. B. Turner-Evans, N. S. Lewis, and H. A. Atwater, Proceedings of the 34th IEEE PVSC, 2009.
- ³Z. Fan, H. Razavi, J. Do, A. Moriwaki, O. Ergen, Y.-L. Chueh, P. W. Leu, J. C. Ho, T. Takahashi, L. A. Reichertz, S. Neale, K. Yu, M. Wu, J. W. Ager, and A. Javey, *Nature Mater.* **8**, 648 (2009).
- ⁴L. Tsakalacos, J. Balch, J. Fronheiser, B. A. Korevaar, O. Sulima, and J. Rand, *Appl. Phys. Lett.* **91**, 233117 (2007).
- ⁵O. Gunawan and S. Guha, *Sol. Energy Mater. Sol. Cells* **93**, 1388 (2009).
- ⁶M. Gloeckler, A. L. Fahrenbruch, and J. R. Sites, Third World Conference on Photovoltaic Energy Conversion, 2003, pp. 491–494.
- ⁷P. J. Sellin, A. W. Davies, A. Lohstroh, M. E. Özsan, and J. Parkin, *IEEE Trans. Nucl. Sci.* **52**, 3074 (2005).
- ⁸L. A. Kosyachenko, A. I. Savchuk, and E. V. Grushko, *Thin Solid Films* **517**, 2386 (2009).
- ⁹S. Mora, N. Romeo, and L. Tarricone, *Nuovo Cimento* **60**, 97 (1980).
- ¹⁰T. Taguchi, J. Shirafuji, and Y. Inuishi, *Jpn. J. Appl. Phys.* **13**, 1169 (1974).
- ¹¹A. M-Acevedo, *Sol. Energy* **80**, 675 (2006).
- ¹²M. J. Kerr, J. Schmidt, and A. Cuevas, *J. Appl. Phys.* **89**, 3821 (2001).
- ¹³M. J. Romero, T. A. Gessert, M. M. Al-Jassim, R. G. Dhere, D.S. Albin, and H. R. Moutinho, *The role of interfaces in thin-film CdTe solar cells*, MRS Symposia Proceedings No. 719 (Materials Research Society, Pittsburgh, 2002), p. F8.40.1–F8.40.6.
- ¹⁴Y. Marfaing, *Thin Solid Films* **387**, 123 (2001).
- ¹⁵H. R. Moutinho, F. S. Hasoon, F. Abulfotuh, and L. L. Kazmerski, *J. Vac. Sci. Technol. A* **13**, 2877 (1995).